

A Stray Light Analysis of the Apache Point Observatory 3.5-Meter Telescope System

Stephen M. Pompea^a, Richard N. Pfisterer^b, and Jeffrey S. Morgan^c

^aNational Optical Astronomy Observatory, Tucson, Arizona¹, ^bPhoton Engineering LLC, Tucson, Arizona², ^cDepartment of Astronomy, University of Washington, Seattle, Washington³

ABSTRACT

A stray light analysis of the Apache Point Observatory 3.5 meter telescope system was done to understand the performance for a variety of imaging modes. The telescope system consists of the 3.5-m telescope, its enclosure, and its associated imaging cameras. The purpose of the study was to assess the stray light performance of this system, identify where modification(s) would improve the system off-axis rejection characteristics, and assess the effectiveness of those modifications. A detailed telescope system geometry model was created, and scatter models were created for telescope and enclosure components. The computer model we created duplicated the pinhole stray light images taken with the telescope, thereby verifying the model. The Point Source Transmittance (PST), a commonly used metric for assessing stray light was used to evaluate the stray light performance of the system for a number of off-axis angles and to suggest modifications to enhance the system.

The baseline PST of the existing system shows virtually no falloff with off-axis angle in the plane of the observatory slit. This is the result of (1) the focal plane having a large, unobstructed view of the Nasmyth mirror and cell, primary mirror cell, and baffles mounted on the Nasmyth cell, (2) relatively unobstructed illumination of telescope over a large range of angles in the plane of the slit, and (3) secondary and Nasmyth baffles that are not enclosed. These attributes create a series of first-level

scatter paths that directly illuminate the focal plane. Our approach to stray light reduction was to address the light paths revealed by the various PST calculations. Our calculations have shown that significant gains can be realized with simple modifications to the telescope system.

1. INTRODUCTION

The role of stray light analysis in improving telescope and telescope system performance has been well-established in space telescopes such as SIRT¹ and in ground-based telescopes such as the Sloan Digital Sky Survey Telescope.² The general approach has been previously summarized for both space systems³ and for ground-based systems with adaptive optics.⁴ Advances in stray light analysis have recently made this approach even more effective for analysis of telescope/instrument systems.⁵ The current computer analysis programs such as *ASAP* and *Fred* can analyze systems of greater complexity and in more detail than previously possible. These advances allow direct comparisons between focal plane stray light analysis images generated using a well-constructed computer model and actual imaging data from point sources. These comparisons can also be used to validate complex stray light models, such as the ones presented in this paper. The current study highlights the effectiveness of stray light studies in generating accurate values of stray light levels, and in describing the spatial variations of stray light across the focal plane.

The University of Washington wished to both improve the stray light rejection of the Apache Point Observatory's 3.5-m telescope when used with the current suite of telescope instrumentation and to evaluate the performance of the telescope if it were to be used with a wide field imaging camera. The proposed camera had a rectangular FOV with an angular coverage of 0.32° X 0.80° when used on the 3.5-m telescope. Hereafter, we will refer to this wide field configuration as the UWBC (UW Big Camera).

This paper describes efforts towards an understanding of the scattered light problems with the current telescope configuration and those that will be encountered with the telescope system incorporating this wide-field imager. The goals of this work were to identify where modifications of the 3.5-m telescope system would improve the off-axis rejection characteristics of the telescope and to assess the effectiveness of those modifications. The main focus of this work was to improve the on-axis performance of the telescope. However, in light of development efforts on the UWBC, a second goal of this project was to evaluate the off-axis

¹ NOAO, 950 N. Cherry Avenue, Tucson, AZ 85719. Also, Adjunct Associate Astronomer, Steward Observatory, University of Arizona. This work was done as a consultant before the author was affiliated with NOAO. Email: spompea@noao.edu

² Photon Engineering, LLC P.O. Box 31316, Tucson AZ 85751. Email: richp@photonengr.com

³ University of Washington, Box 351580, Seattle WA, 98195. Email: morgan@astro.washington.edu

scattering for a wide field of view system and to make sure that the suggested modifications will not impede the performance of the wide-field system. A key aspect of this study is the attention given to stray light as a system issue, involving the telescope, enclosure, camera, and operations.

There were four stages to this effort. First, the model of the telescope system was constructed, briefly illustrated in Figures 1-3. We used the prescription of the optical system, a description of all coatings used in the optical system, and drawings of the current support structures and baffles to construct a model. This model included the optical properties of all mechanical structures on the telescope itself and even the optical properties of the observing floor, the telescope enclosure, and the catwalk which allows service personnel access to the top of the telescope structure. The catwalk consists of an open grate floor and its associated railings on three sides of the telescope at about the level of the telescope secondary when the telescope is pointed toward the zenith. For the purpose of validating this telescope model, we obtained a set of stray light pinhole measurements from the telescope.

The second stage was to compare the results from our computer model with on-axis measurements in order to both understand the limitations of the model and to improve it. The goal of this second stage of work was to produce model estimates of both the average level of scattered light and contour plots showing the variation of scattered light within the field of view of the Seaver Prototype Imaging camera (SPICam), a general purpose direct imaging CCD camera. It contains a backside illuminated SITE 2048x2048 pixel device with 24-micron pixels and a plate scale of 0.14 arcseconds per pixel, giving a field of view of 4.78 arcminutes. The model estimates of stray light levels were made for several off-axis angles for a point source.

The third stage of this effort was to use the model to evaluate the stray light rejection characteristics of the telescope under variable conditions. These calculations were used to determine off-axis angles instructive to the stray light performance of the system and to suggest modifications to the telescope baffling. The suggested modifications considered ranged from simple modifications of the present design to a complete redesign of the baffle system. An important part of the third stage of this effort was to evaluate what effects the proposed baffling modifications will have on the UWBC's field of view. For this evaluation, model estimates of the stray light across the UWBC's field of

view in two orientations of the instrument rotator were made. For each rotator position, we computed the stray light level before and after the suggested baffling modifications. These calculations were done at a reduced spatial resolution for angles of interest of the off-axis source.

2. COMPUTER MODEL OF SYSTEM GEOMETRY AND SCATTER CHARACTERISTICS

In order to be effective, computer modeling of telescope systems must be accurate and sufficiently detailed. In particular, the surface scatter characteristics of the surfaces in the system, including mirror, baffle, and various other system surfaces must be well-known. Efforts in the US and Canada to establish databases of the scatter properties of surfaces⁶ have greatly aided this effort, as have reviews of the measured scatter properties of surfaces.⁷ A summary of optical models and measurements of black surfaces is given in the *Handbook of Optics* chapter on this topic⁸ and is particularly useful for black baffle surface modeling. Similarly, realistic optical models of mirror surfaces in the observatory environment must also be constructed. Stray light modeling software allows the selection of simple scatter models or the construction of more complex scatter models based on bidirectional reflectance scatter distribution function (BRDF) measurements at a particular wavelength.

We constructed models of about 50 surfaces of the telescope system, including the gray linoleum that comprises the observing floor. Of greatest importance were models of black baffle surfaces such as the ones coated with Aeroglaze Z-306. The BRDF model of Aeroglaze Z-306 used in the model was based upon actual measurements and is shown in Figure 4. On the x-axis is plotted $\log_{10} |\sin \theta - \sin \theta_0|$, where θ and θ_0 are the scatter and specular angles measured from the surface normal. On the y-axis we plot the \log_{10} of the BRDF for this coating.

Since the BRDF of an ideal Lambertian scatterer is a constant for all angles, this data indicates that the scatter from Aeroglaze is not Lambertian. The data shows an increasing forward-scatter component that means that significant amounts of power will be scattered at larger angles of incidence.

The mirror surfaces were assigned composite models to represent both specular and scatter characteristics. Since the particulate deposition rates in observatories are not well-studied, we would have preferred to have the mirror surfaces examined and particulate counts made in

order to properly model the scatter properties of the contaminated surfaces.

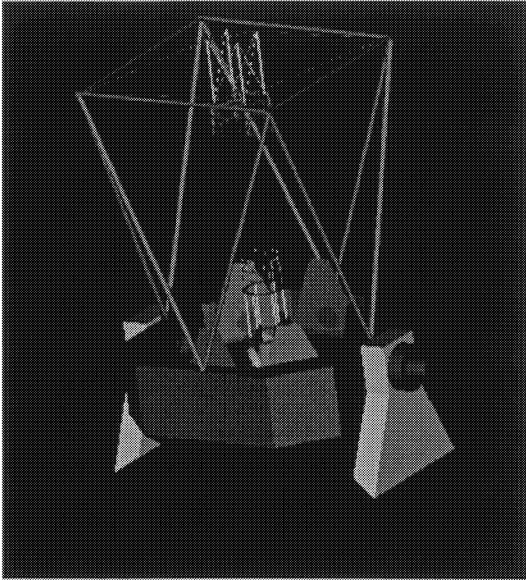


Figure 1 Apache Point 3.5-meter Telescope Model. A similar model of the enclosure was made.

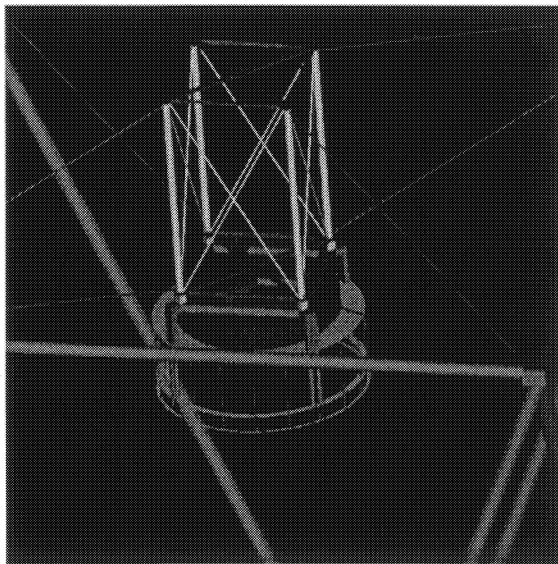


Figure 2 View of Secondary Mirror and Support Structure

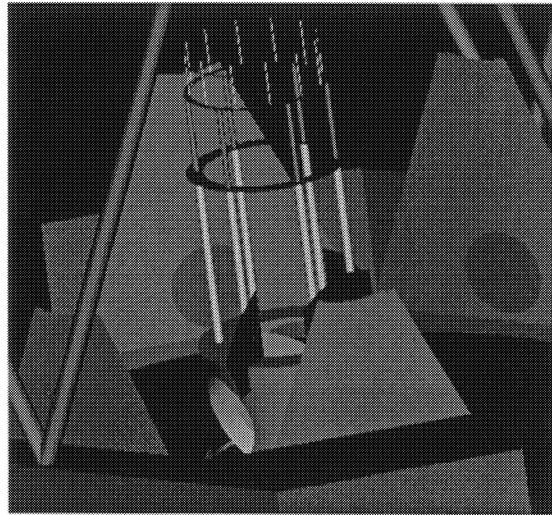


Figure 3 View of Nasmyth Fold Mirror and Baffles

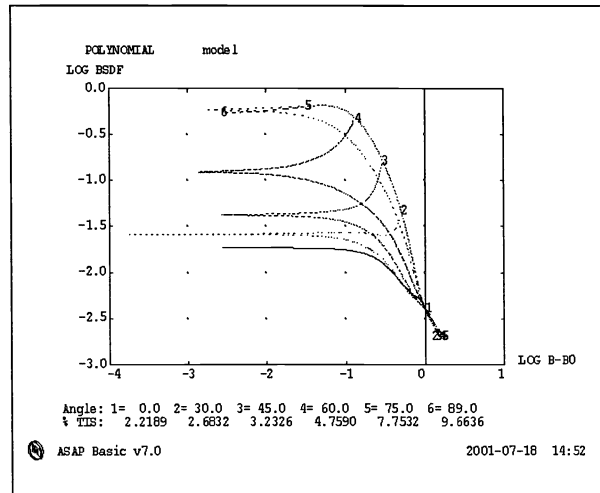


Figure 4 BRDF Model of Aeroglaze Z-306

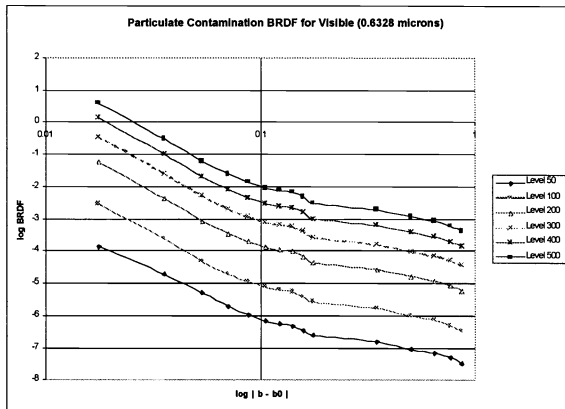


Figure 5 BRDF Models for Particulate Contamination for Levels 50 (top) to 500 (bottom)

Lacking specific information, we decided to use the MIL-1246B particulate model commonly used in industry⁹ shown in Figure 5. This model is traceable, well-known, and often used in studies of this type. Its major drawbacks are (1) it tends to overestimate the number of particles (at least relative to cleanroom measurements) and is therefore conservative and (2) as with any generic model, it may not represent our specific case.

The cleanliness level of the mirror is determined by exposure; the longer the surface is exposed to the environment, the “dirtier” it becomes. Since the telescope mirrors are cleaned on a regular basis, we expect significant variation in particulate count over time. Taking a conservative approach, we assumed level 500 particulates; a surface at this level of contamination is visibly “dirty” (i.e., the observer can see particles on the surface) but only 0.3% of the surface is actually obscured with particles.

3. MODEL VERIFICATION USING PINHOLE IMAGERY

Pinhole images taken with the Apache Point telescope on 7 January 2001 for verification of and comparison with the computer model were used. The images were taken at the telescope focal plane. At a distance of 118.0 inches from the axis of the Nasmyth fold mirror (3.05 inches from the focal plane), a pinhole aperture was placed in the optical path. A 400 micron diameter aperture was used for the observations and in our model. The optical path consisted of the primary, secondary, and Nasmyth fold mirrors; no other camera lenses were placed in the optical path for these photographs.

The moon and Jupiter, shining at magnitudes -12.94 and -2.7 , respectively, were visible during this observing session and were considered the most significant out-of-field light sources. They represent the illuminating sources in the observations. Using tables of right ascension and declination coordinates of the moon and Jupiter during the observing session, as well as elevation and azimuth angles describing the pointing of the telescope, we converted the lunar and Jovian coordinates into altitude and zenith distance angles, and then converted these data into a format convention understood by the stray light modeling program.

Figures 6-9 show the actual and simulated images. Telescope images are labeled en01.009, en01.011, en01.013, and en01.017. The computer model shows excellent agreement with the actual pinhole images. A sophisticated use of the current generation of stray light software tools such as BRO’s ASAP program and Photon Engineering’s FRED program, allows these comparisons to be made. Previously, this type of comparison and agreement has been difficult if not impossible to achieve.

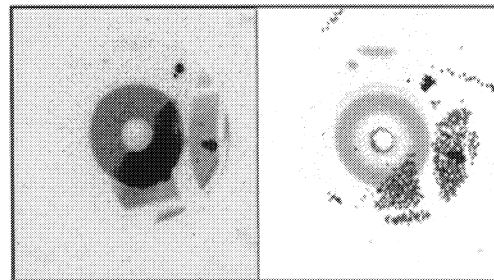


Figure 6 Actual (left) and Simulated (right) EN01.009 Images. Telescope 1 degree north of Jupiter.

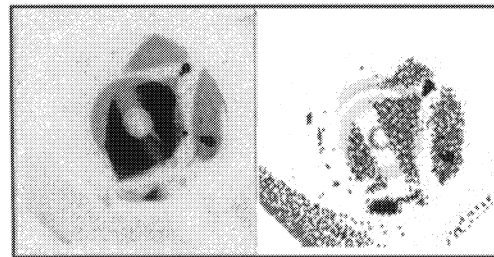


Figure 7 Actual (left) and Simulated (right) EN01.011 Images. Telescope 2 degrees north of Jupiter.

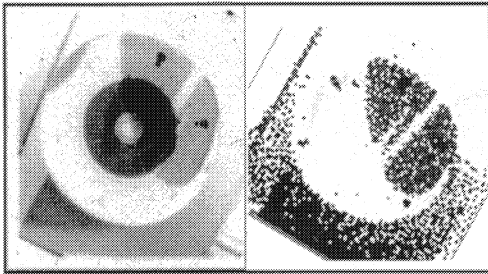


Figure 8 Actual (left) and Simulated (right) EN01.013 Images (A power threshold settings was responsible for the missing image of the primary mirror in the simulated image.) Telescope 30 degrees north of Jupiter.

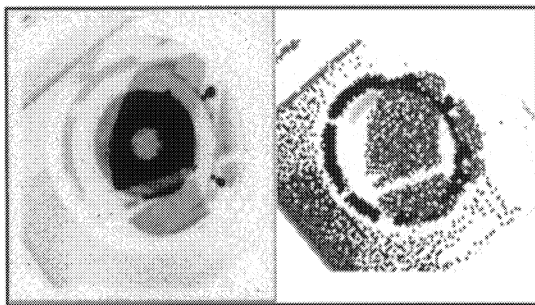


Figure 9 Actual (left) and Simulated (right) EN01.017 Images (A power threshold settings was responsible for the missing image of the primary mirror in the simulated image.) Telescope 4 degrees north of Jupiter.

3. PST ANALYSES OF EXISTING THE OBSERVATORY CONFIGURATION

The Point Source Transmittance (PST) is a commonly used metric for assessing the stray light characteristics of an opto-mechanical system. The PST does not attempt to identify source(s) of stray light but instead combines all stray light mechanisms into a single number that is convenient for comparing systems and enhancements.

More specifically the PST is a transfer function relating the irradiance at the focal plane due to stray light mechanisms to the irradiance at the entrance aperture of the telescope produced by a distance point source, viz.

$$PST(\theta) = \frac{\text{focal plane irradiance}}{\text{entrance aperture irradiance}(\theta)}$$

This definition is particularly applicable to systems with obscured or varying apertures. There are other PST definitions based upon power ratios, but they are much less appropriate for obscured systems.

For our PST calculations of the existing observatory configuration, we made the following assumptions:

1. The entrance aperture irradiance is unity. Since this appears in the denominator of the PST equation, it is a convenient normalization.
2. The focal plane is 4 inches in diameter. This is a smaller focal plane than was used for the pinhole image calculations. For the sake of these calculations, it is not important if the focal plane is an array or continuous surface.
3. The baffle we labeled “NA 2 Baffle Rot” baffle with an aperture 3.08 inches in diameter was removed from model. This baffle is only used for the pinhole observations and calculations.
4. The telescope is rotated to 0 degrees azimuth (telescope pointing south), 60 degrees elevation position from the horizontal.
5. Relative to the nominal telescope pointing, the PST is calculated over the range from -60 degrees to +60 degrees in the “elevation” direction. This is referred to as the “elevation PST scan”. The telescope is not moved, but the source is moved about the static telescope.
6. Relative to the nominal telescope pointing, the PST is calculated over the range from -70 degrees to +70 degrees in the “side-to-side” direction. The “side-to-side” direction is perpendicular to the elevation direction and passes through the nominal telescope pointing at 60 degree elevation.
7. PST calculations are performed with slit and telescope housing in place so obscurations are properly accounted for.

The stray light analysis generated PST curves for a variety of situations. These curves are especially instructive as they give the baseline telescope performance. As shown in Figure 10, the nominal PST in the elevation direction is relatively flat as a function of angle. The only real “feature” is the on-axis peak due to near-specular Lorentzian scatter from the mirror surfaces. At high elevation angles we observe some rolloff from transmission/blockage of light through the catwalk.

In the “side-to-side” scan (Figure 11), the PST drops off with negative angle (i.e., the point source is moving west, away from the Nasmyth fold mirror) because of

the shadowing of mirror by the telescope slit. In the positive angle direction (i.e., the point source is moving east), the Nasmyth fold mirror and associated structures are illuminated and can scatter directly into the focal plane. Consequently the PST stays high until the telescope slit blocks the illumination.

The constant PST indicates that the telescope performance is not optimized for stray light. To diagnose the cause of these relatively constant PST values, we need to consider how stray light propagates through system. Workers in this stray light field typically consider two classes of structures:

“illuminated” objects and “critical” objects.

“Illuminated” objects are those objects directly or indirectly (i.e., by reflection) illuminated by the point source. “Critical” objects are those objects that can be seen either directly or indirectly (i.e., by reflection) by the focal plane. If a structure is simultaneously illuminated by the point source and can be seen by the focal plane, then we have a potentially significant stray light path. It is a “potential” stray light path because the structure in question must have a scatter function that radiates energy into the direction of the focal plane in order to transfer energy.

The structures of the telescope are largely exposed to the point source over the entire elevation PST scan and so virtually every objects can be considered an “illuminated” object.

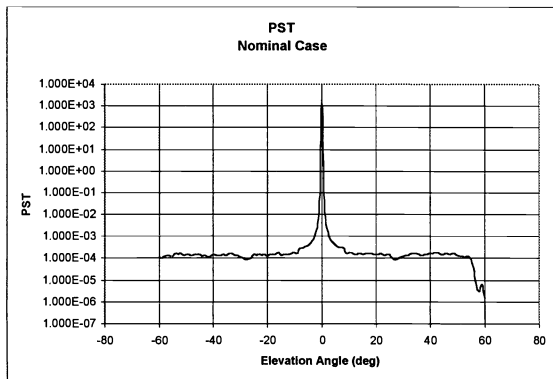


Figure 10 Elevation PST for Existing Observatory Configuration

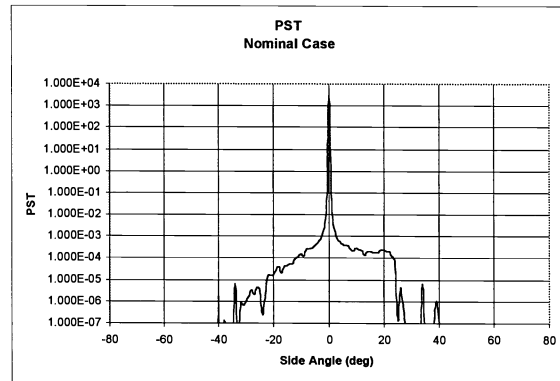


Figure 11 Side PST for Existing Observatory Configuration

In order to determine what the focal plane can see, we can trace rays from the focal plane backward through the system and note which structures are intersected. Ideally the focal plane would only see the surfaces of the Nasmyth fold mirror, secondary and primary mirrors. However as shown in Figure 12, the focal plane can see the Nasmyth mirror and cell, portions of the primary mirror cell, planar baffles mounted on top of the Nasmyth mirror cell (called in the model the “3RY NA Baffles”), and the last annulus of the primary mirror baffle. Figure 12 was generated prior to adding the primary mirror petal covers to the model, which is why they are missing.

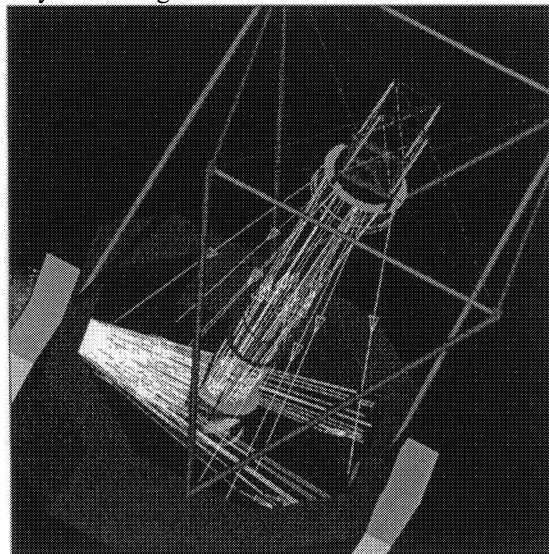


Figure 12 Tracing Rays Backwards from the Focal Plane to Identify “Critical” Objects

The focal plane can certainly see several of the petals as well. Since these structures are always seen by the focal plane and they are almost always illuminated by the point source, the system has a first-level scatter path that does not drop off with angle. Therefore, the elevation PST stays relatively constant with angle.

For comparison, we isolated the scatter contributions from the three mirrors and plotted their PST with the complete system PST. These are shown in Figures 13 and 14. Our goal was to assess the relative magnitude of the stray light relative to ubiquitous mirror scatter. Within the field-of-view, mirror scatter must be tolerated because the focal plane must look through the optics to see the object being observed. Outside the field-of-view, the Lorentzian scatter function drops with angle until the optics are shadowed and no longer directly illuminated by the point source. In this case however the optics are illuminated over a broad range of elevation angles and so we observe only the Lorentzian falloff.

In the absence of a main telescope baffle (“telescope tube”), these PST calculations indicate the minimum amount of stray light that can be achieved for a given level of mirror quality and contamination.

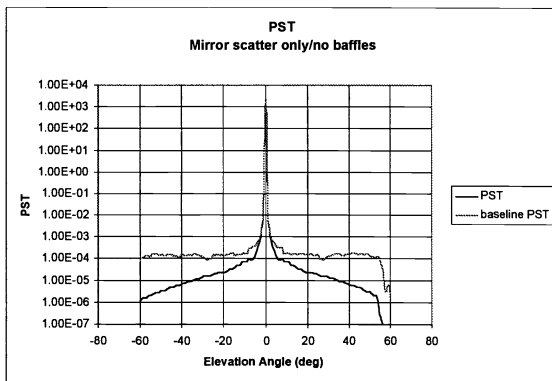


Figure 13 Elevation PST for Existing Observatory Configuration with Mirror Scatter Isolated and Shown for Comparison

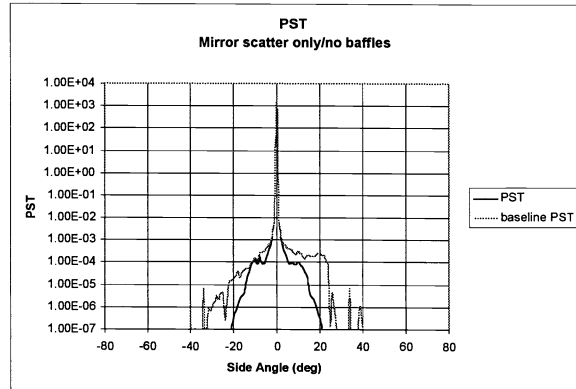


Figure 14 Side PST for Existing Observatory Configuration with Mirror Scatter Isolated and Shown for Comparison

Value of an Annular Baffle

Upon examination of the baseline PST and the backward ray traces, it is clear that limiting the field-of-view of the focal plane could reduce the stray light levels. Ideally the focal plane should only see the optical surfaces, but this is not practical in most systems, particularly those without a relay between first focus and the final image. Consequently the best we could do is to insert some new limiting aperture between the focal plane and the Nasmyth fold mirror. Raytracing the FOV corresponding to the 4 inch diameter focal plane we decided to employ a 7.6 inch inner diameter baffle at the primary mirror cell. (See Figure 15) This is the smallest aperture we could use without vignetting the FOV.

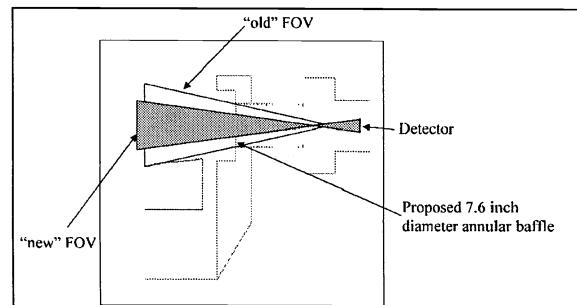


Figure 15 Limiting the FOV of the Focal Plane Detector with a New Annular Baffle

Figures 16 and 17 show the PST scans with the annular baffle. For comparison we plotted the baseline and “mirrors only” PST scans as well. It is clear that adding the baffle has the effect of reducing the elevation PST,

dropping it an order of magnitude at ± 60 degrees off-axis.

The annular baffle also eliminates the asymmetry in the side PST scan by blocking a scatter path from the Nasmyth mirror mount. Since the proposed annular baffle is straightforward to implement (a “simple fix”), we added it to the model for all subsequent calculations.

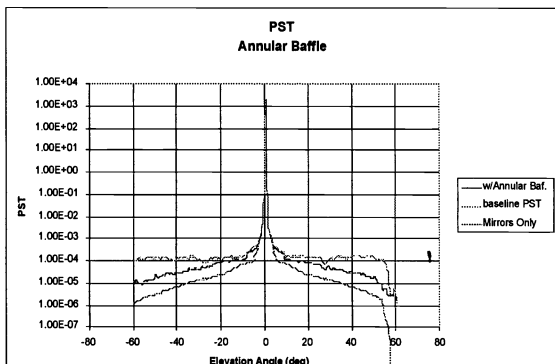


Figure 16 Elevation PST w/Annular Baffle (Mirror scatter and baseline shown for comparison.)

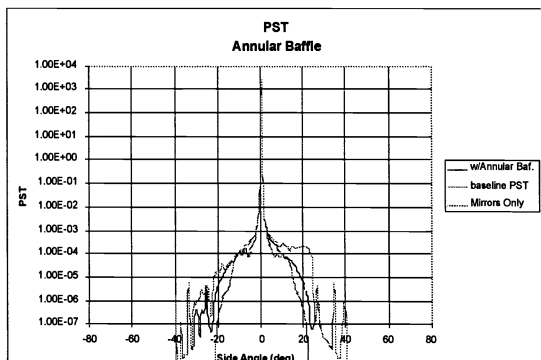


Figure 17 Side PST w/Annular Baffle (Mirror scatter and baseline shown for comparison.)

Value of a Slit Windscreen

The previous PST calculations lead to the conclusion that the observatory slit is an effective stray light baffle in the side-to-side direction because it shadows the telescope. In the elevation direction however the telescope can be illuminated over a large range of angles. This suggests that an effective baffle strategy would be to close off the slit except where it needs to be open for the telescope FOV.

Figure 18 shows the potential addition of a slit windscreen above and below the telescope’s FOV.

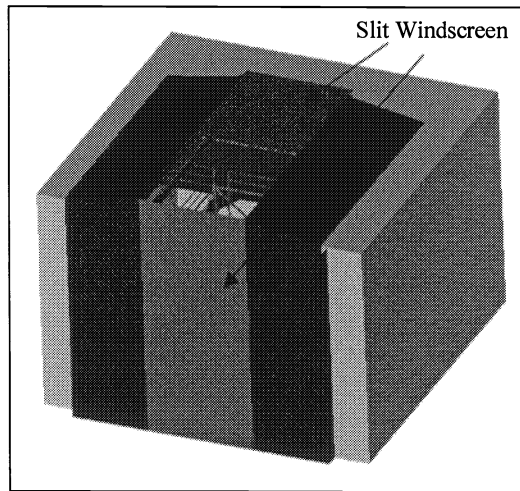


Figure 18 Observatory w/Slit Windscreen

Figures 19 and 20 show the PST scans with the slit windscreen in place. (Recall that the previously discussed annular baffle is also included in the model.) Compared to the baseline (existing) observatory configuration, these two modifications (annular baffle and slit windscreen) significantly reduce the elevation PST. The asymmetry in the elevation PST is due to the placement of the slit windscreens. Notice that the slit windscreen has no effect on the side PST scan.

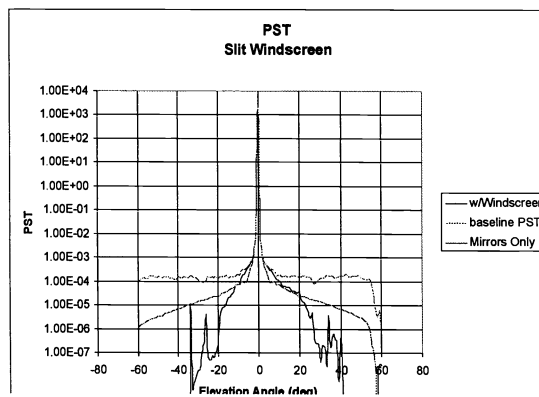


Figure 19 Elevation PST w/Slit Windscreen (Mirror scatter and baseline shown for comparison.)

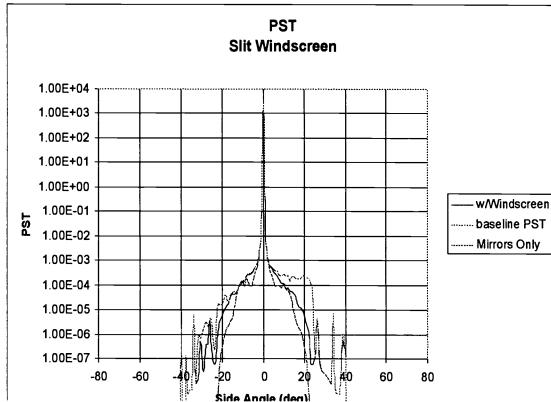


Figure 20 Side PST w/Slit Windscreen (Mirror scatter and baseline shown for comparison.)

Value of North and South Shrouds

Given the power of the modeling program, we investigated the value of another approach by making minor modifications to the model. With the goal of shadowing the primary mirror and the Nasmyth fold mirror mounting, another alternative is to surround the main truss with an opaque material that can act as a telescope “tube”.

Enclosing the main truss would upset the airflow around the telescope and so we looked at the effect of covering only the north and south sides of the main truss with an opaque structure. In our model we assumed that this opaque structure was black on both sides with a BRDF similar to that of Aeroglaze Z-306.

It is interesting to note that, while the north and south shrouds reduce the PST relative to the baseline (existing) configuration, they do not do as well as the slit windscreen. The reasons for this are twofold: (1) the slit windscreen is physically farther from the telescope and so it casts a shadow at a smaller off-axis angle (effectively shadowing the telescope at approximately ± 20 -25 degrees off-axis) and (2) the black shroud can itself scatter light.

Since the shroud is not present in the side-to-side direction, it is not surprising that our results showed that it has no effect on the PST in that direction.

Modifications To The Secondary And Nasmyth Baffles

In its unbaffled form, the image plane in a Cassegrain telescope is exposed to out-of-field stray light that bypasses the secondary mirror and enters the central

hole in the primary mirror. The common solution to this problem has been to implement a conical baffle around the secondary mirror and a second conical baffle extending from the primary mirror.

In the design of these baffles, the usual strategy is to adjust the dimensions and locations of the baffles to block the “limiting ray”, that is, the ray that intersects the edge of the secondary mirror baffle, the open aperture of the primary conical baffle, and the edge of the image plane itself. In practice most designers select a point somewhat away from the edge of the image plane to allow for tolerances.

It turns out that there are an infinite number of solutions for the dimensions and locations of the two conical baffles that block the limiting ray. However the optimal solution is often the arrangement of effective baffles that also present the least amount of obscuration to the incoming light. Several years ago one of us (RP) developed software that determines these optimum baffle dimensions and locations. Table 1 gives the parameters of the baffles as computed by our software for a “protected” image plane diameter of 4.2 inches.

Table 1 Optimum Baffle Parameters*

Baffle	Z Location (inches)	Semi-diameter (inches)
Primary or Nasmyth	89.800	10.263
Secondary	184.971	16.311

*Z location is relative to the primary mirror vertex

To block grazing incidence reflections from the side wall of the primary baffle, it is generally considered a good practice to add vanes along the length. After deciding that two vanes could be reasonably effective, we computed vane inner diameters that wouldn't vignette the imaging rays from the edge of the 4-inch diameter field. Table 2 gives the vane parameters.

Table 2 Primary or Nasmyth Vane Parameters**

Vane	Z Location (inches)	Aperture Semi-diameter (inches)
1	69.800	9.427
2	49.800	8.576

** Z location is relative to the primary mirror vertex

It was also clear from our experience that the use of better optical black surfaces than Aeroglaze Z-306 could enhance the stray light properties of the system. The use of a black-flocked surface as a more optimal treatment for the surfaces of the baffles has been explored in various projects by one of us (SP). Such an optically rough surface can have a total hemispherical reflectivity of approximately 1.2% in the visible. To put this into perspective, Martin Black, an excellent black surface treatment for aluminum often used in space telescopes, has a total hemispherical reflectivity at significantly higher.) Furthermore black-flocked surfaces have a significantly lower forward scatter BRDF at larger incidence angles than most paints, which behave badly at larger angles of incidence.

After reviewing the black-flocked surface BRDF data, we decided to represent these secondary and Nasmyth baffle surface as a Lambertian scattering surface with a total hemispherical reflectivity of 1.5%. This model gave us a sense of how good the baffle performance could be if the optimal black surfaces are chosen.

Figures 21 and 22 show the PST scans with the secondary and Nasmyth baffles in place, with the improved coating. (Recall that the previously discussed annular baffle is also included in the model.) In the elevation scan, the optimized baffles appear to reduce the PST by over an order of magnitude; however by comparing with previous PSTs, we note that half of the improvement is due to annular baffle. Therefore relative to the existing more open annular rings and support tubes, these enclosing baffles are about a factor of 3 times better. In the side PST scan, there is a more subtle improvement, when this PST is compared to previous PST measurements.

4. CONCLUSIONS

A detailed computer model of the Apache Point observatory has been developed from CAD drawings. After assigning scatter models to the various components, we duplicated pinhole images taken with the telescope with the computer model, thereby verifying the model.

The baseline PST of the existing system shows virtually no falloff with off-axis angle in the plane of the observatory slit. This is the result of (1) the focal plane having a large, unobstructed view of the Nasmyth mirror and cell, primary mirror cell, and baffles mounted on the Nasmyth cell, (2) relatively unobstructed illumination of

telescope over a large range of angles in the plane of the slit, and (3) secondary and Nasmyth baffles that are not enclosed. These attributes create a series of first-level scatter paths that directly illuminate the focal plane.

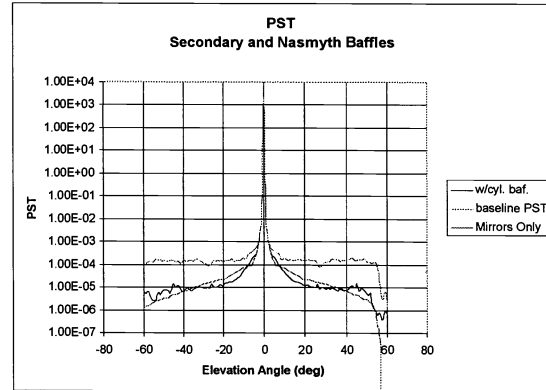


Figure 21 Elevation PST w/Secondary and Nasmyth Baffles (Mirror scatter and baseline shown for comparison.)

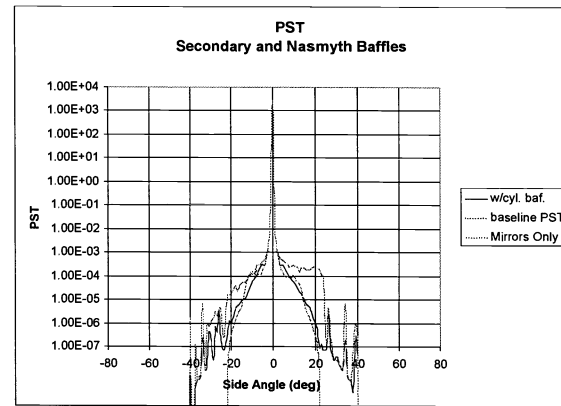


Figure 22 Side PST w/ Secondary and Nasmyth Baffles (Mirror scatter and baseline shown for comparison.)

Our approach to stray light reduction was to address each issue separately. To reduce the FOV of the focal plane, we proposed a simple annular baffle at the primary mirror cell. To reduce the illumination of the telescope, we proposed installing a slit windscreen, which was responsible for a dramatic drop in the PST. We also analyzed the value of shrouds on the north and south sides of the main truss, which is a less practical approach and less effective because the black surfaces can scatter. Finally we proposed replacing the annular rings and support tubes with enclosing secondary and Nasmyth baffles. With optimal low scatter surfaces on

these baffles, the PST can drop by approximately a factor of 3. Significant overall improvements are possible through these system modifications.

The analysis presented here relies heavily upon having a model of the complete telescope/instrument/enclosure system to use in stray light calculations. Note that applying best practices or "rules of thumb" in stray light control might allow one to improve the system. However, the systematic improvement of the system can best be achieved through a modeling-based approach which provides the necessary tools to understand system performance and to experiment with system modifications. The use of a systematic modeling-based approach allows one to assess the system performance in a quantitative way and to reduce the most severe stray light problems first. As solutions to these problems are found, other stray light reduction opportunities present themselves and can be sequentially addressed. Stray light reduction and system performance improvement, deserve to be addressed seriously with the software tools and approaches presented here, whether they are done early in a system design or to a mature, operating system.

5. REFERENCES

- ¹ D. W. Bergener, S. M. Pompea, D. F. Shepard, and R. P. Breault, "Stray Light Rejection Performance of SIRTf: A Comparison", *Proceedings of the SPIE: Stray Radiation IV.*, 511 (1984) 64.
- ² S. M. Pompea, J. E. Mentzell, and W. E. Siegmund, "A Stray Light Analysis of the Sloan Digital Sky Survey Telescope", *Proceedings of the SPIE: Stray Light IV*, 1753 (1993).
- ³ S. M. Pompea, "The Management of Stray Radiation Issues in Space Optical Systems", *Space Science Reviews*, 74: 181-193, (1995).
- ⁴ S. M. Pompea, "Stray Radiation Issues in Astronomical Systems with Adaptive Optics", *Adaptive Optics for Astronomy*, Kluwer Academic Publishers, 1995.
- ⁵ S. M. Pompea, "Advances in the Stray Light Analysis of Astronomical Telescope Systems", *Proceedings of the SPIE: Optical Telescopes of Today and Tomorrow: Following in the Direction of Tycho Brahe*, A. Arneberg, Editor, 2871, 193-195, (1997).
- ⁶ S. McCall, R. L. Sinclair, S. M. Pompea, and R. P. Breault, "Spectrally Selective Surfaces for Ground and Space-Based Instrumentation: Support for a Resource

Base", *Proceedings of the SPIE: Space Astronomical Telescopes and Instruments II*, 1945 (1993).

⁷ S. H. C. P. McCall, S. M. Pompea, R. P. Breault, and N. L. Regens, "Reviews of Black Surfaces", *Proceedings of the SPIE: Stray Light IV*, 1753 (1993). Reprinted in *Selected Papers on Cryogenic Optical Systems*, Gerald R. Pruitt, Editor, SPIE Milestone Series, 1994.

⁸ S. M. Pompea and R. P. Breault, [Invited chapter] "Optical Black Surfaces", in *Handbook of Optics*, 2nd edition, Optical Society of America, 2000.

⁹ Spyak, P., Wolfe, W., "Scatter from particulate-contaminated mirrors. part 4: properties of scatter from dust for visible to far-infrared wavelengths", *Optical Engineering*, Vol. 31, No. 8, August 1992, pp.1775-1784.

ASAP is a proprietary product of Breault Research Organization, Inc., Tucson, AZ.

RhinoCad is a proprietary product of Robert McNeel & Associates, Seattle, WA.

Fred is a proprietary product of Photon Engineering LLC, Tucson AZ.